Electromagnetic-mechanical-thermal fully coupled model for Terfenol-D devices

Wenmei Huang,[1,2,a)] Zhangxian Deng,[2] Marcelo J. Dapino,[2] Ling Weng,[1] and Bowen Wang[1]
[1]*Key Laboratory of Electro-Magnetic Field and Electrical Apparatus Reliability of Hebei Province, Hebei University of Technology, Tianjin 300130, China*
[2]*Department of Mechanical and Aerospace Engineering, The Ohio State University, Columbus, Ohio 43210, USA*

(Presented 7 November 2014; received 22 September 2014; accepted 23 November 2014; published online 6 April 2015)

This paper presents a fully coupled, nonlinear electromagnetic-mechanical-thermal model for Terfenol-D devices which include active magnetostrictive materials and passive components. The model includes two parts: (1) a material-level discrete energy-averaged model (DEAM) to describe the magnetomechanical coupling and thermal effect of Terfenol-D and (2) a system-level finite element model formulated in weak form using Maxwell's equations, Newton's law, and heat transfer equations. The objective is to describe the electromagnetic, mechanical, and thermal dynamics of the device. The system finite element model is constructed in COMSOL Multiphysics, and the nonlinear behavior of Terfenol-D is coupled through lookup tables generated by the DEAM. Preliminary results of the output capacity of a Terfenol-D actuator with respect to ambient temperature are presented in terms of blocked force, free displacement, and output power. The blocked force and free displacement decrease by 8.0% and 29.8%, respectively, for a 12 A (RMS) excitation current, as the temperature increases from 20 °C to 180 °C. One of the key contributions of this study is that it accounts for both the temperature-dependent Terfenol-D properties and the thermal effects of surrounding passive systems. © *2015 AIP Publishing LLC*. [http://dx.doi.org/10.1063/1.4916810]

Magnetostrictive terbium-iron-dysprosium alloys (Terfenol-D) exhibit strong coupling between magnetic and mechanical energies. Terfenol-D generates giant magnetostriction (∼1600 ppm) combined with a large energy coupling factor (∼0.75) and fast dynamic response (∼20 kHz).[1] Hence, Terfenol-D can be used in applications such as sonar transducers, ultrasonic devices, linear motors, and micropumps and microvalves.[1,2] A typical Terfenol-D device consists of active magnetostrictive materials and surrounding passive components, including a magnetic path for flux completion, a structural load transmission, permanent magnets for biasing, and a copper coil for generating a magnetic field.

Experiments[3–6] have shown that Terfenol-D devices exhibit frequency-dependent hysteresis and electromagnetic-mechanical-thermal coupling nonlinear behaviors. Models for magnetostrictive materials and devices include the Jiles-Atherton model, Preisach model, Armstrong model, and their extended models, but most of these models assume a constant operating temperature. Recently, Wang and Zhou[7] proposed a nonlinear transient constitutive model for Terfenol-D using a lumped parameter method. They included higher order terms in the Gibbs energy expansion, and used a Langevin function to describe the nonlinear magnetization-field relationship and temperature dependence. But this approach does not consider the structural dynamic behavior arising from device operation.

Evans and Dapino[8] proposed an accurate and computationally efficient model, which considers local energies near Galfenol's six easy crystallographic directions. Chakrabarti and Dapino[9] implemented this material-level model and developed a 3D fully coupled, anhysteretic, finite element (FE) model. Deng and Dapino[10] later added material hysteresis to the 3D FE framework. However, both FE models only consider coupling of the electromagnetic and mechanical domains: the thermal field is not included. This paper extends the framework to encompass electromagnetic, mechanical, and thermal domains by adding another independent variable, T_{emp}. This fully coupled FE model is implemented in COMSOL Multiphysics. The primary aim of the model is to describe the system level input-output relationships, for optimal design and accurate control of practical magnetostrictive devices.

At the system level, magnetostrictive devices exhibit coupling between the material's constitutive relation and the device's structural dynamics. Most prior work has focused on the one-way or two-way coupling between magnetic and mechanical domains. Notwithstanding, thermal dynamics should also be considered, especially for devices working in alternating current or stress. The fully coupled relations in the electromagnetic-mechanical-thermal multi-field in magnetostrictive devices are schematically illustrated in Fig. 1. The dashed lines denote the effects of one-way coupling that have been considered in the literature. The solid lines need to be added to create a fully coupled system-level model for magnetostrictive devices. This study specifically considers thermal effects and thermal expansion.

The discrete energy average model (DEAM) for magnetostrictive materials has been described in Refs. 8–10. The DEAM assumes the bulk behavior of magnetostrictive

a)Author to whom correspondence should be addressed. Electronic mail: huzwm@hebut.edu.cn.

materials is a weighted sum of local responses which are determined by local Gibbs energies. The local Gibbs energy function, based on the sum of magnetocrystalline anisotropy, magnetoelastic, and magnetic field energy terms, is defined as

$$G^k = w^k G^k_{A0} + \frac{1}{2}K^k|\mathbf{m}^k - \mathbf{c}^k|^2 - \mathbf{S}^k_m \cdot \mathbf{T} - \mu_0 M_s \mathbf{m}^k \cdot \mathbf{H}, \quad (1)$$

where k denotes the number of easy directions, the anisotropy constant K^k controls how steep the anisotropy energy wells are around the *kth* easy axis $\mathbf{c}^k$, and $\mathbf{m}^k$ is the moment orientation, $\mathbf{S}^k_m$ is the magnetostriction, M_s is the saturation magnetization, $\mathbf{T}$ is the stress tensor, and $\mathbf{H}$ is the magnetic field vector. Here, G^k_{A0} is the global anisotropy energy, which for materials with cubic anisotropy is given by

$$G^k_{A0} = K_4[(m^k_1 m^k_2)^2 + (m^k_2 m^k_3)^2 + (m^k_3 m^k_1)^2] + K_6(m^k_1 m^k_2 m^k_3)^2; \quad (2)$$

G^k_{A0} is weighted by w^k, an empirical weighting factor that adjusts the anisotropy energy along the *kth* easy axis. The orientations of Terfenol-D moments are calculated through minimization of (1). Assuming $||\mathbf{m}^k|| \approx \mathbf{c}^k \cdot \mathbf{m}^k = 1$, the analytical solution for moment orientations $\mathbf{m}^k$ can be written as

$$\mathbf{m}^k = (\mathbf{K}^k)^{-1}\left[\mathbf{B}^k + \frac{1 - \mathbf{c}^k \cdot (\mathbf{K}^k)^{-1}\mathbf{B}^k}{\mathbf{c}^k \cdot (\mathbf{K}^k)^{-1}\mathbf{c}^k}\mathbf{c}^k\right], \quad (3)$$

where the magnetic stiffness matrix $\mathbf{K}^k$ and force vector $\mathbf{B}^k$ are

$$\mathbf{K}^k = \begin{bmatrix} K^k - 3\lambda_{100}T_1 & -3\lambda_{111}T_4 & -3\lambda_{111}T_6 \\ -3\lambda_{111}T_4 & K^k - 3\lambda_{100}T_2 & -3\lambda_{111}T_5 \\ -3\lambda_{111}T_6 & -3\lambda_{111}T_5 & K^k - 3\lambda_{100}T_3 \end{bmatrix}, \quad (4)$$

$$\mathbf{B}^k = [c_1K^k + \mu_0 M_s H_1 \;\; c_2K^k + \mu_0 M_s H_2 \;\; c_3K^k + \mu_0 M_s H_3]^T. \quad (5)$$

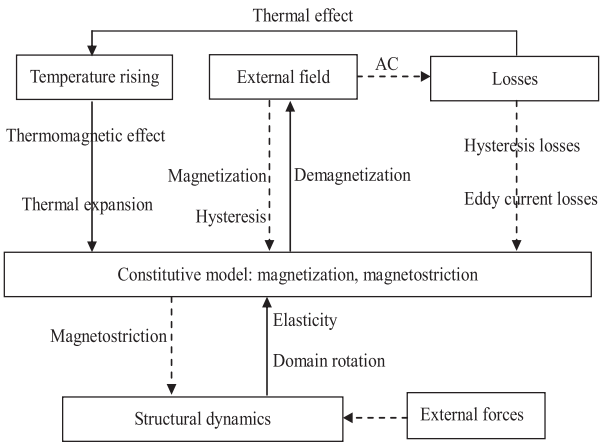

FIG. 1. Multi-field fully coupled relations in magnetostrictive devices.

TABLE I. Saturation magnetostriction (from Ref. 6).

Pressure (MPa) \ Temperature (°C)	20	60	100	140	180
20	1830	1680	1620	1525	1380
40	1920	1820	1715	1620	1465
60	1970	1872	1776	1678	1510
80	2006	1900	1805	1692	1525

The bulk magnetization $\mathbf{M}$ and strain $\mathbf{S}$ are the weighted sum of the magnetization $M_s\mathbf{m}^k$ and the magnetostriction $\mathbf{S}^k_m$ due to each orientation[8]

$$\mathbf{M} = M_s \sum_{k=1}^{r} \xi^k_{an}\mathbf{m}^k, \quad \mathbf{S} = s\mathbf{T} + \sum_{k=1}^{r} \xi^k_{an}\mathbf{S}^k_m. \quad (6)$$

As detailed in Ref. 8, ξ^k_{an} is the volume fraction of the *kth* orientation.

The existing DEAM is a magnetic-mechanical coupled model. This study adds temperature dependence through three aspects: saturation magnetization M_s, saturation magnetostriction λ, and thermal expansion.

It has been proposed that for ferromagnetic materials[11] the saturation magnetization M_s depends on temperature T_{emp} according to the relation

$$M_S(T_{emp}) = M_s\left(\frac{T_{empc} - T_{emp}}{T_{empc} - T_{empr}}\right)^x, \quad (7)$$

where T_{emp} stands for the ambient temperature, T_{empc} is the Curie temperature, and T_{empr} is the spin reorientation temperature. We assume that $T_{empc} = 380\,^\circ\text{C}$, $T_{empr} = 0\,^\circ\text{C}$, and $x = 0.5$ for Terfenol-D.

Experimental results show that the saturation magnetostriction $\lambda(T, T_{emp})$ of Terfenol-D is a function of temperature T_{emp} and compressive stress T. Table I shows the saturation magnetostriction data for different temperatures and stresses.[6] In this study, a 2D interpolation function is applied to describe the data in Table I.

In order to incorporate thermal expansion with the existing DEAM, a linear term αT_{emp} is added to calculate the bulk strain

$$S = sT + \alpha T_{emp} + \sum_{1}^{r} \xi^k_{an}S^k_m. \quad (8)$$

The thermal expansion coefficient α varies between 4 and 12 ppm/°C (Ref. 12). In this study, $\alpha = 5$ ppm/°C. This study implements the DEAM to generate interpolation functions (lookup tables) for COMSOL Multiphysics v4.4. The material properties, which have been proven accurate in previous research,[9] are listed in Table II.

TABLE II. Terfenol-D material properties used in this study.

Parameter	Value	Parameter	Value
K^k	13.652e5	w^3-w^4	0.85277
K_4	−0.06e6	w^5-w^8	0.58886
K_6	−0.2e6	E_s	115e9
w^1-w^2	1.3389		

The response of Terfenol-D devices can be described using three physical domains: electromagnetic, structural mechanics, and thermal. The weak form of Maxwell's electromagnetic equation and Newton's equation can be written as (Ref. 8)

$$\int_{V_B} \mathbf{H} \cdot \delta\mathbf{B} dV + \int_{V_B} \boldsymbol{\sigma} \frac{\partial \mathbf{A}}{\partial t} \cdot \delta\mathbf{A} dV = \int_{\partial V_B} (\mathbf{H} \times \mathbf{n}) \cdot \delta\mathbf{A} d\partial V + \int_{V_B} \mathbf{J}_s \cdot \delta\mathbf{A} dV, \quad (9)$$

$$\int_{V_u} \mathbf{T} \cdot \delta\mathbf{S} dV + \int_{V_u} \left(\rho \frac{\partial^2 \mathbf{u}}{\partial t^2} + c \frac{\partial \mathbf{u}}{\partial t} \right) \cdot \delta\mathbf{u} dV = \int_{\partial V_u} \mathbf{f}_A \cdot \delta\mathbf{u} d\partial V + \int_{V_u} \mathbf{f}_B \cdot \delta\mathbf{u} dV, \quad (10)$$

where $\mathbf{B}$ is the flux density, $\mathbf{A}$ is the vector magnetic potential, $\mathbf{n}$ is the normal vector of the boundary surface, $\mathbf{J}_s$ is the current density, and $\boldsymbol{\sigma}$ is the material conductivity; $\mathbf{u}$ is the displacement field, ρ is the material density, c is the damping coefficient, $\mathbf{f}_A$ is the traction, and $\mathbf{f}_B$ is the body force; V_B and V_u are the solution domain of the electomagnetic and mechanical field, respectively.

For the thermal field, using the temperature $\mathbf{T}_{emp}$ as independent variable, the mathematical model for heat transfer by conduction is

$$\rho C_p \frac{\partial \mathbf{T}_{emp}}{\partial t} - \nabla \cdot (k_c \nabla \mathbf{T}_{emp}) = \mathbf{Q}, \quad (11)$$

where C_p is the heat capacity, k_c is the thermal conductivity tensor, and Q is the heat source. Adopting Galerkin's method, we multiply (11) by an arbitrary weighting function $\mathbf{v}$, and integrate over the solution domain (volume V_T enclosed by surface ∂V_T) to obtain

$$\int_{V_T} \left[\rho C_p \frac{\partial \mathbf{T}_{emp}}{\partial t} - \nabla \cdot (k_c \nabla \mathbf{T}_{emp}) - \mathbf{Q} \right] \cdot \mathbf{v} dV_T = 0. \quad (12)$$

Integration by parts yields the weak form of thermal domain

$$\int_{V_T} k_c \nabla \mathbf{T}_{emp} \cdot \nabla \mathbf{v} dV_T + \int_{V_T} \rho C_p \frac{\partial \mathbf{T}_{emp}}{\partial t} \cdot \mathbf{v} dV_T = \int_{\partial V_T} k_c \nabla \mathbf{T}_{emp} \mathbf{n} \cdot \mathbf{v} d\partial V_T + \int_{V_T} \mathbf{Q} \cdot \mathbf{v} dV_T. \quad (13)$$

Weak forms (9), (10), and (13) are set up and solved in COMSOL Multiphysics v4.4. The nonlinear constitutive behavior of Terfenol-D is coupled through lookup tables generated by the DEAM.

In order to validate the proposed model, a 2D axisymmetric Terfenol-D actuator geometry is built in COMSOL Multiphysics v4.4. The actuator consists of a Terfenol-D rod 13.335 mm in diameter and 25.4 mm in length, an output piston, an excitation coil with 485 turns, and a low carbon steel case for the magnetic circuit.

A previous study presented a FEM model based on lookup tables for magnetostrictive systems, whose magnetic field H and magnetostriction λ are uniaxial.[13] Similar lookup tables incorporating temperature dependence are generated using the new DEAM developed. The nonlinear behavior of Terfenol-D is described using interpolation functions $H(B, T, T_{emp})$ and $\lambda(B, T, T_{emp})$, which are functions of flux density B, stress T, and temperature T_{emp}. The performance of a Terfenol-D actuator is quantified in COMSOL Multiphysics for different initial conditions, boundary conditions, and driving currents.

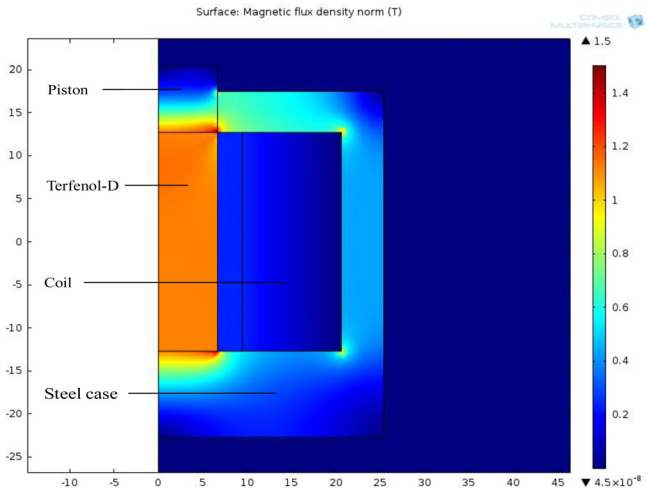

FIG. 2. 2D axisymmetric Terfenol-D actuator and flux density distribution in COMSOL.

Figure 2 shows the 2D axisymmetric actuator geometry and the flux density distribution when the excitation current is 10 A, the temperature is 20 °C, and the prestress is 0 MPa. It is observed that the flux density in the Terfenol-D driver is approximately homogeneous with an average value of 1.14 T.

Figure 3 displays the magnetostriction versus quasi-static magnetic field at different temperatures, at 16.6 MPa fixed prestress. The calculated results are consistent with the experimental data.[6] The mean-square-root derivation is 5.26 ppm and the maximum relative error is 2.17%. Both magneto-mechanical coupling (magnetic domain rotation)

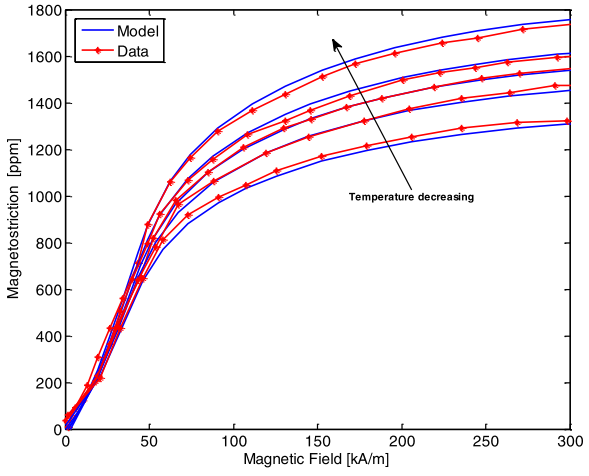

FIG. 3. Magnetostriction vs. quasi-static magnetic field at different temperatures (20 °C, 60 °C, 100 °C, 140 °C, and 180 °C), at 16.6 MPa fixed prestress.

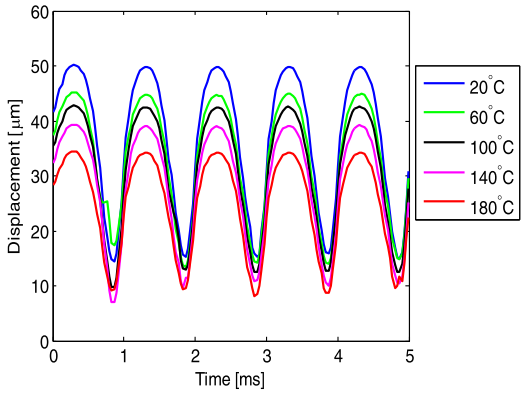

FIG. 4. System output displacement at different temperatures.

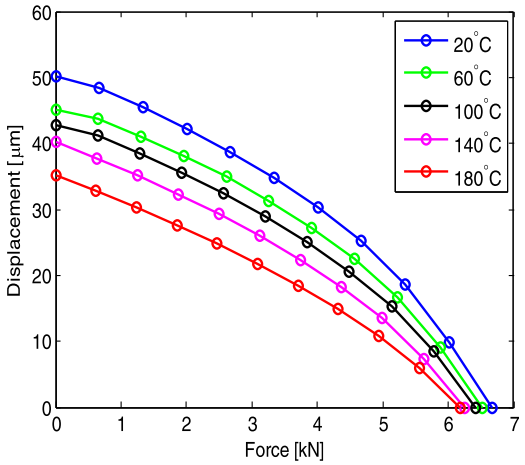

FIG. 5. Load lines of the actuator at different temperatures.

and temperature T_{emp} influence the shape of the H-λ curves. When the prestress is fixed, the magnetic moment rotation is the main contribution to magnetostriction at a low magnetic field, and the influence of temperature-dependent saturation magnetostriction is relatively weak. Hence, the H-λ curves for different temperatures overlap each other at low magnetic fields. As the magnetic field increases, Terfenol-D tends to saturate and temperature influence starts to dominate at high magnetic fields, as shown in Fig. 3. The higher the temperature is, the lower the magnetostriction.

The model also describes the dynamic response of the actuator system. Figure 4 shows the output displacement of the actuator under no load for a 1 kHz, 6 A amplitude sinusoidal AC driving current, with a 6 A DC bias. The five time traces have different bias operating points due to different $B(H, T, T\text{emp})$ property curves at different temperatures. Thus, the traces are shifted from upper to lower positions with the temperature increase. The peak-to-peak value of the output displacement decreases by 34.6% (from 35.41 μm at 20 °C to 23.16 μm at 180 °C). This result quantifies the degree by which increasing temperature reduces the performance of Terfenol-D devices.

A parametric sweep of load force applied on the piston is used to study the power output capability of the actuator. Under no load (zero force produced), the actuator's displacement is maximized (free displacement), while the actuator's ability to generate force is maximized as the strain produced tends to zero. This maximum force (blocked force) of the actuator depends on its stress state, its temperature, and the magnetic field applied to it. The blocked force and free displacement of the actuator at different temperatures with a 12 A (RMS) excitation current are shown in Fig. 5. With increasing temperature, the blocked force decreased by 8.0% (from 6731.72 kN at 20 °C to 6194.24 kN at 180 °C) and the free displacement decreased by 29.8% (from 50.21 μm at 20 °C to 35.22 μm at 180 °C). This result quantifies the degree by which the system's performance decreases with increasing temperature.

This paper presented a fully coupled, 2D electromagnetic-mechanical-thermal finite element model for Terfenol-D devices. Weak form equations derived from Maxwell's equations for electromagnetic system, Newton's equation for mechanical systems, and heat transfer equations for thermal systems were implemented in COMSOL Multiphysics v4.4. A constitutive model of Terfenol-D considering temperature dependence was constructed based on the existing DEAM. Material nonlinearities exhibited by Terfenol-D were described by lookup tables created by the proposed DEAM in COMSOL Multiphysics, thus achieving higher computational efficiency. Output capability in terms of block force and free tip displacement was quantified at different temperatures. One of the key contributions of this study is that both the temperature-dependent Terfenol-D properties and the thermal effects of surrounding passive systems were taken into account.

We wish to acknowledge financial support from the National Natural Science Foundation of China (Grant Nos. 51171057 and 51201055) and from the Natural Science Foundation of Hebei Province (Grant No. E2014202246), and from the University Innovation Team Leader Program of Hebei Province (LJRC003).

[1]F. T. Calkins, R. C. Smith, and A. B. Flatau, IEEE Trans. Magn. **36**, 429 (2000).
[2]A. Grunwald and A. G. Olabi, Sens. Actuators, A **144**, 161 (2008).
[3]A. E. Clark, J. P. Teter, and O. D. McMasters, J. Appl. Phys. **63**, 3910 (1988).
[4]F. T. Calkins, M. J. Dapino, and A. B. Flatau, Proc. SPIE **3041**, 293 (1997).
[5]A. Clark and D. Crowder, IEEE Trans. Magn. **21**, 1945 (1985).
[6]Y. R. Liang and X. J. Zheng, Acta Mech. Solida Sin. **20**, 283 (2007).
[7]T. Wang and Y. Zhou, J. Appl. Phys. **108**, 123905 (2010).
[8]P. G. Evans and M. J. Dapino, J. Appl. Phys. **107**, 063906 (2010).
[9]S. Chakrabarti and M. J. Dapino, J. Appl. Phys. **111**, 054505 (2012).
[10]Z. X. Deng and M. J. Dapino, J. Intell. Mater. Syst. Struct. **26**, 47 (2015).
[11]A. Raghunathan, Y. Melikhov, J. E. Snyder, and D. C. Jiles, IEEE Trans. Magn. **46**, 1507 (2010).
[12]M. A. Jiboory and D. G. Lord, IEEE Trans. Magn. **26**, 2583 (1990).
[13]Z. X. Deng and M. J. Dapino, Proc. SPIE **9057**, 90572A (2014).